Cell Communication and Signaling

RESEARCH

Open Access

Deficiency of GCN5 exacerbates pulmonary fibrosis by disrupting the LKB1–AMPK pathway

Seunghee Byun[1], Hyunsik Kim[1], Sun-Ho Lee[1], Jae-Hwan Kwon[1], Hyunseung Kim[1], Myung Hyun Sohn[2], Hyo Sup Shim[3], Moo Suk Park[4], Chun Geun Lee[5,6], Jack A. Elias[6], Jung-Yoon Yoo[7], Soo-Yeon Park[1*] and Ho-Geun Yoon[1*]

Abstract

Background Idiopathic pulmonary fibrosis (IPF) is a fatal and progressive respiratory disease characterized by aberrant epithelial remodeling, excessive extracellular matrix (ECM) deposition, and fibroblast activation. Although LKB1-AMPK signaling axis is known to suppress epithelial-to-mesenchymal transition (EMT) and lung fibrosis, the upstream regulatory mechanisms governing this pathway remain unclear. General control non-depressible 5 (GCN5) is a lysine acetyltransferase that modulates protein function and cellular pathways via acetylation, but its contribution to lung fibrosis has not been investigated.

Methods To investigate the role of GCN5 in pulmonary fibrosis, we analyzed publicly available transcriptomic datasets from IPF patients. GCN5 expression was validated in lung tissues from IPF patients and mouse fibrosis models (lung-specific TGF-β_1 transgenic and bleomycin-treated mice) using immunohistochemistry. Protein-protein interactions between GCN5 and LKB1 were assessed by co-immunofluorescence in mouse tissues and in vitro translation followed by immunoprecipitation. LKB1 acetylation sites were identified using in silico docking system and functionally validated by site-directed mutagenesis. GCN5 knockdown and overexpression were performed in lung epithelial cells to examine downstream signaling. To evaluate therapeutic potential, GCN5-expressing adenovirus was delivered intratracheally to bleomycin-treated mice.

Results Here, we revealed a significantly reduced expression of GCN5 in lung tissues from both patients with IPF and lung fibrosis mouse models. Notably, GCN5 directly bound to liver kinase B1 (LKB1), a master regulator of AMP-activated protein kinase (AMPK), and acetylated LKB1 lysine residues at its C-terminal region. In particular, GCN5-mediated LKB1 acetylation at lysine 431 (K431) enhanced LKB1 kinase activity. GCN5 knockdown in lung epithelial cells reduced LKB1 acetylation at K431, leading to decreased AMPK phosphorylation and subsequent promotion of EMT. Conversely, GCN5 overexpression reversed transforming growth factor-beta–induced profibrotic phenotype. Furthermore, adenovirus-mediated overexpression of GCN5 alleviated fibrosis in bleomycin-treated mice.

*Correspondence:
Soo-Yeon Park
SOOYEONP@yuhs.ac
Ho-Geun Yoon
YHGEUN@yuhs.ac

Full list of author information is available at the end of the article

Conclusions Our findings identify GCN5 as a novel upstream regulator of the LKB1–AMPK signaling in lung epithelial cells. GCN5 deficiency in fibrotic conditions reduces LKB1 acetylation and disrupts epithelial homeostasis, facilitating EMT and fibrosis progression. Restoring GCN5 expression rescues this signaling axis and mitigates fibrosis, highlighting its potential as a therapeutic target of IPF.

Keywords GCN5, LKB1, AMPK, Pulmonary fibrosis, Epithelial-to-mesenchymal transition, TGF-β

Graphical Abstract

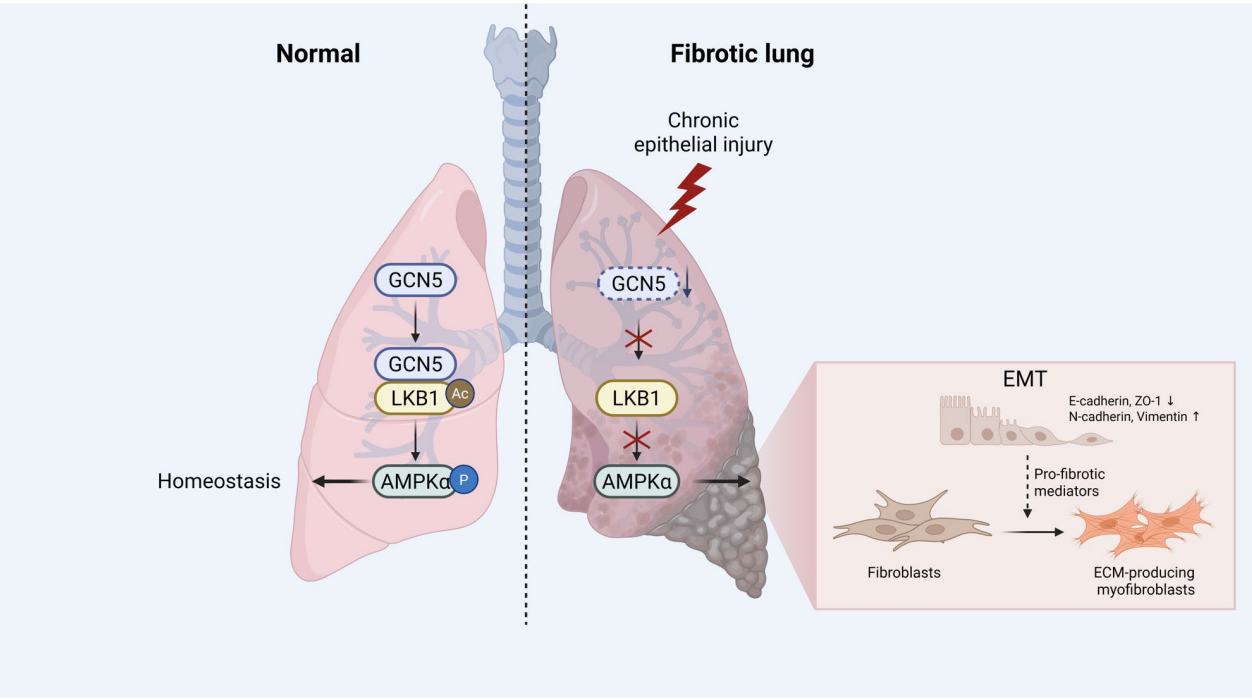

Introduction

Idiopathic pulmonary fibrosis (IPF) is a chronic interstitial lung disease characterized by an unknown etiology and poor clinical outcome. Patients with IPF commonly experience dyspnea, dry cough, and reduced exercise tolerance, which significantly affect their quality of life [1, 2]. Current research paradigms indicate that repetitive lung epithelium injury triggers a pathogenic cascade that culminates in differentiation into matrix-producing myofibroblasts. Excessive extracellular matrix (ECM) deposition causes irreversible lung tissue scarring and impairs respiratory function [3, 4]. Despite ongoing research, a comprehensive understanding of the biological mechanisms driving IPF remains incomplete, highlighting the urgent need for further studies to identify the key regulatory factors involved in fibrosis progression.

The pathogenesis of IPF involves multiple cellular and molecular processes. The key mechanisms implicated in the development of IPF include epithelial-to-mesenchymal transition (EMT), chronic inflammation, and fibrocyte recruitment [5–7]. Among these, EMT is a biological process in which epithelial cells lose their polarity and cell–cell adhesion properties. Subsequently, they acquire mesenchymal characteristics, including enhanced migratory capacity and increased ECM production [8]. In the context of IPF pathogenesis, persistent lung epithelial injury is considered a primary initiating factor for EMT, wherein damaged lung epithelial cells downregulate epithelial markers, such as E-cadherin and ZO-1, while upregulating mesenchymal markers, including N-cadherin, Vimentin, and ZEB1 [9–11]. Bronchial and alveolar epithelial cells have been reported to undergo EMT and adopt fibroblast-like characteristics in response to transforming growth factor-beta (TGF-β) stimulation [12–14]. EMT-derived cells do not fully transdifferentiate into fibroblasts; however, they actively support the formation of a pro-fibrotic microenvironment through paracrine signaling [15]. They secrete various cytokines and growth factors that stimulate resident fibroblasts and increase ECM remodeling. This epithelial–mesenchymal crosstalk creates a self-perpetuating loop that reinforces fibrotic responses in the affected tissue [16]. Furthermore, epithelial cells that undergo EMT exhibit increased expression of fibrosis markers such as collagen and connective tissue growth factor [17].

Several pathophysiological processes are implicated in the regulation of EMT and fibrosis, including the AMP-activated protein kinase (AMPK), Notch, PI3K/Akt, and TGF-β signaling pathway [18, 19]. Among these, AMPK activation has been associated with the suppression of fibrotic responses. For instance, AMPK activation inhibits TGF-β–induced fibroblast activation, thereby reducing collagen accumulation [20–23]. Liver kinase B1 (LKB1 or STK11) is a major upstream activator of AMPK [24] and is essential for maintaining cellular energy balance and regulating cell proliferation [25–27]. LKB1 dysregulation has been implicated in fibrosis and tumorigenesis [28–30], with its inactivation promoting EMT through ZEB1 upregulation, thus facilitating invasion and metastasis in lung cancer [29]. In addition, LKB1 downregulation in alveolar epithelial cells impairs autophagy and induces EMT [28].

The activity of LKB1 is intricately controlled by various post-translational modifications [31–34]. Although LKB1 phosphorylation has been extensively investigated in various diseases [35, 36], LKB1 acetylation and its biological significance remain elusive. Considering the crucial role of LKB1 in AMPK activation and fibrosis suppression, identifying the regulatory mechanisms of its acetylation may provide novel insights into the pathogenesis of pulmonary fibrosis.

General control non-depressible 5 (GCN5 or KAT2A) is a core member of the GCN5-related N-acetyltransferase (GNAT) family and functions as the catalytic component of the Spt-Ada-GCN5 acetyltransferase complex, which is essential for transcriptional regulation via chromatin remodeling [37, 38]. GCN5 exhibits both histone acetyltransferase (HAT) and lysine acetyltransferase (KAT) activity. As an acetylation regulator, GCN5 plays crucial roles in cancer, metabolic disorders, and inflammatory diseases by contributing to a wide range of biological processes [39–41]. While the pathological role of other HATs, such as p300 and CBP, has been extensively documented in pulmonary fibrosis [42–46], the specific function of GCN5 remains unknown. Therefore, elucidating the pathophysiological role of GCN5 is crucial for uncovering molecular mechanisms underlying pulmonary fibrosis.

In this study, we demonstrated the antifibrotic role of GCN5 and its regulatory effect on LKB1 acetylation in pulmonary fibrosis. We observed that GCN5 expression was significantly downregulated in fibrotic lungs. GCN5 downregulation reduces LKB1 acetylation, thereby decreasing AMPK phosphorylation and increasing EMT, contributing to fibrosis progression. In contrast, GCN5 overexpression attenuated pulmonary fibrosis in both in vitro and in vivo models. These findings suggest that GCN5 is a novel regulator of pulmonary fibrosis and highlight its potential as a therapeutic target for IPF.

Methods

Human samples

Human lung samples were obtained from the tissue bank at Severance Hospital (Seoul, Korea). Tissues from the normal lung portions of patients with lung cancer were used as control samples in this study. Patients with IPF fulfilled the diagnostic criteria established by the American Thoracic Society and the European Respiratory Society, and the diagnosis of IPF was supported by history, physical examination, pulmonary function studies, and chest high-resolution computed tomography.

Mouse models

All animal experiments were approved by the Yonsei University College of Medicine Institutional Animal Care and Use Committee (IACUC No. 2023-0025). Eight-week-old C57BL/6 male mice (Orient Bio, Korea) were used as lung injury models. The mice were anesthetized intraperitoneally with Zoletil (50 mg/mL) and Rompun (23.32 mg/mL), followed by an intratracheal injection of 2 mg/kg of bleomycin (BLM; sc-200134 A; Santa Cruz Biotechnology, USA) with a 30-gauge needle. The control group received the same volume of saline. Lung tissue samples were collected 14 days after BLM instillation. To induce TGF-β_1 overexpression, 8-week-old TGF-β_1 transgenic mice (*Ccsp-rtTA-tTs-TGF-β_1*) and littermate controls were randomized to normal or 0.5 mg/mL of doxycycline (DOX)-containing water [47]. DOX administration was maintained for 4 weeks, and the mice were then sacrificed. To induce GCN5 overexpression in mice, Ad5-GCN5-HA (2.0×10^{11} VP) was administered via intratracheal injection. Lung tissues and bronchoalveolar lavage (BAL) fluid were collected 8 days post injection. In vivo viral infection was confirmed by the expression of green fluorescence in the lung tissue. The mice were housed in a specific pathogen-free condition and 12-h light/dark cycle conditions.

Cell culture and reagents

The human bronchial epithelial cell line BEAS-2B (CRL-3588; ATCC, USA) was maintained in RPMI1640 (10-040-CV; Corning Inc., USA) medium supplemented with 10% fetal bovine serum (FBS) (35-015-CV; Corning Inc., USA) and 1% antibiotic–antimycotic solution at 37℃ under 5% CO_2. The mouse bronchial epithelial cell line C22 (Sigma-Aldrich, USA) was maintained in permissive conditions (Dulbecco's Modified Eagle's Medium [DMEM; 10-013-CV; Corning, USA] supplemented with 2% FBS, penicillin [100 U/mL], streptomycin [100 μg/mL], endothelin-1 [0.25 μg/mL], insulin [10 μg/mL], transferrin [5 μg/mL], endothelial cell growth supplement [7.5 μg/mL], epidermal growth factor [0.025 μg/mL], hydrocortisone [0.36 μg/mL], and T3 [0.02 μg/mL] at 33℃ under 5% CO_2). RLE-6TN, HEK293FT cells were

cultured in DMEM. Cells were transferred to the serum-free medium and subjected to starvation for 2 h. Subsequently, 20 ng/mL of TGF-β_1 (CYT-716; ProSpec, Israel) was added, and the cells were collected 24 h later.

Immunoprecipitation (IP) and western blotting

The cells were washed with ice-cold phosphate-buffered saline (PBS) and collected. Cell pellets were lysed in lysis buffer (50 mM Tris-HCl, 150 mM NaCl, 0.2% Triton X-100, 1.5% $MgCl_2$, 0.3% NP-40, 1 mM ethylene glycol tetraacetic acid, and 1 mM ethylenediaminetetraacetic acid [EDTA]) supplemented with a protease inhibitor cocktail (P3100-020; GenDEPOT, USA) and phosphatase inhibitors (200 mM Na_3VO_4 and 200 mM NaF) on ice for 30 min. The lysates were cleared by centrifugation at 13,000 rpm for 15 min at 4℃. Protein concentration was determined using a 660-nm protein assay reagent (22660; Thermo Fisher Scientific, USA).

For immunoprecipitation, lysates were precleared by incubation with protein A/G beads at 4℃ for 1 h with gentle rotation. The beads were removed by centrifugation at 3,500 rpm for 3 min. The precleared lysates were incubated with the primary antibody at 4℃ for 2 h. Protein A/G beads were prewashed three times with lysis buffer before being added to the lysate–antibody mixture. After overnight incubation at 4℃, the beads were washed five times with lysis buffer to remove unbound proteins. The immunoprecipitated complexes were eluted by boiling with sodium dodecyl sulfate sample buffer at 95℃ for 5 min. For negative controls, mouse IgG was used under identical immunoprecipitation conditions.

Equal amounts of whole-cell extract and immunoprecipitated eluates were separated with polyacrylamide gel electrophoresis and transferred to polyvinylidene difluoride membranes (IPVH00010; Merck, Germany). The membranes were blocked with 5% nonfat milk in PBS containing Tween-20 (PBST) at room temperature for 2 h and then probed with primary antibodies. The following antibodies were used: anti-GCN5 (3305; Cell signaling, USA), anti-LKB1 (sc-32245; Santa Cruz Biotechnology, USA), anti-phospho-LKB1 (sc-271924; Santa Cruz Biotechnology, USA), anti-Flag M2 (F3165, Sigma-Aldrich, USA), anti-Myc (2278; Cell signaling, USA), anti-HA (3724; Cell signaling, USA), anti-β-actin (A5441; Sigma-Aldrich, USA), anti-phospho-AMPKα T172 (2535; Cell signaling, USA), anti-Acetylated-Lysine (9441; Cell signaling, USA), anti-E-cadherin (3195; Cell signaling, USA), anti-ZO-1 (61-7300; Invitrogen, USA), anti-N-cadherin (13116; Cell signaling, USA), anti-Vimentin (sc-32322; Santa Cruz Biotechnology, USA), anti-α-SMA (ab5694; Abcam, UK), anti-Col1a1 (72026; Cell signaling, USA), and anti-Acetylated-LKB1 K431 (Abfrontier, USA). After three washes with PBST, the membranes were incubated with horseradish peroxidase (HRP)-conjugated secondary anti-rabbit or anti-mouse antibody at 25℃ for 1 h. Chemiluminescence signals were detected and visualized using the LAS-3000 system (Fujifilm, Stanford, CT, USA).

Molecular docking of GCN5 with LKB1

Using the primary sequence of the protein, the three-dimensional (3D) structure was generated with AlphaFold 3 (https://alphafoldserver.com) [48]. Knowledge-based protein–protein docking of GCN5 with LKB1 was performed with the Easy interface of the HADDOCK 2.2 (High Ambiguity-Driven biomolecular DOCKing) webserver [49]. HADDOCK (https://wenmr.science.uu.nl) considers experimental data to drive the molecular docking process, unlike ab initio docking protocols that use only the coordinates of structures [50]. The docking strategy followed by HADDOCK involves three steps: (1) randomization of molecular orientations followed by energy minimization to remove steric clashes, (2) torsion angle dynamics using torsion angles as degrees of freedom, and (3) refinement in an explicit solvent using Cartesian space. A total of 200 clusters obtained from HADDOCK were assessed for interactions between GCN5 and LKB1 using PyMOL. The protein–protein interactions were analyzed on PDBePISA, which was employed to identify interacting interfaces, hydrogen bonds, Gibbs free energy (ΔGint, kcal/mol), salt bridges, non-bonded contacts, tunnels, and pores of the complex. Finally, binding affinity was calculated from the PRODIGY online server (https://wenmr.science.uu.nl/prodigy/) [51], and the binding affinity scores are provided in Supplementary Table 2.

Immunostaining

For immunohistochemistry (IHC), lung sections were deparaffinized and rehydrated through gradient ethanol. Antigen retrieval was performed using citrate-based antigen-unmasking solution (H3300-250; Vector Laboratories, USA) at 95℃ for 10 min and blocked with blocking buffer (S2023; Dako, USA) at room temperature. After blocking, the slides were incubated with the following primary antibodies: anti-GCN5 (sc-365321; Santa Cruz Biotechnology, USA) and anti-α-SMA (ab5694; Abcam, UK). The expression level was identified using the HRP-conjugated secondary antibody (K5007; Dako, USA) for 1 h at room temperature, followed by 1 min of 3,3'-Diaminobenzidine (DAB) solution (SK-4100; Vectorlab, USA) and hematoxylin counterstaining.

Sample preparation for immunofluorescence (IF) was identical to that of IHC until the application of the primary antibodies. The primary antibodies used included anti-GCN5 (sc-365321; Santa Cruz Biotechnology, USA), anti-LKB1 (NBP1-87817; Novus Biologicals, USA), anti-N-cadherin (13116; Cell Signaling, USA), anti-N-cadherin (33-3900; Invitrogen, USA), anti-Col1a1 (72026;

Cell Signaling, USA), anti-SPC (sc-518029; Santa Cruz Biotechnology, USA), anti-CCSP (sc-9773; Santa Cruz Biotechnology, USA), and anti-ZO-1 (61-7300; Invitrogen, USA). The secondary antibodies used were DyLight 488 anti-mouse (DI-2488; Vectorlab, USA) and DyLight 549 (DI-1549). The slides were mounted with 4′,6-diamidino-2-phenylindole (DAPI)-containing mounting medium (ab104139; Abcam, UK) and stored at 4℃ in the dark. A Zeiss LSM780 confocal laser-scanning microscope was used for obtaining and analyzing the images.

For immunocytochemistry (ICC), BEAS-2B cells were fixed with 4% paraformaldehyde for 20 min at room temperature and washed three times with PBS. The cells were then permeabilized using 0.3% Triton X-100 for 15 min and blocked with 3% bovine serum albumin for 30 min. After overnight incubation with primary antibodies at 4℃, the cells were washed with PBS and incubated with a solution containing secondary antibodies for 1 h at room temperature.

In vitro acetylation assay

GST-fused LKB1 proteins were purified from *Escherichia coli* BL21 (DE3) transformed with pGEX-4T1. *E. coli* were induced with 0.5 mM isopropyl-β-D-thiogalactopyranoside (I6758; Sigma-Aldrich, USA) for 20 h at 16℃. The cells were lysed by sonication in lysis buffer (40 mM HEPES, 100 mM KCl, 0.2 mM EDTA, 5 mM $MgCl_2$, 0.1% Nonidet P-40, 10% glycerol, 1.5 mM dithiothreitol, and protease inhibitor cocktail). The GST-tagged recombinant proteins were purified using glutathione-agarose resin (Peptron, Korea). The purified proteins were incubated with in vitro translated GCN5 using a TNT T7 Quick Coupled Transcription/Translation kit (L1170; Promega, UK) at 4℃. The bound proteins were eluted and subjected to immunoblotting analysis with anti-Acetylated-Lysine antibody (9441; Cell Signaling, USA).

RNA extraction and quantitative reverse transcription–polymerization chain reaction (qRT-PCR)

RNAiso Plus (9109; Takara, Japan) was used to isolate total RNA from mouse lung tissue and cells, following the manufacturer's protocol. A NanoDrop 2000 spectrometer (Thermo Fisher Scientific) was used to measure RNA concentration and purity, while the CellScript reverse transcription kit (CDS-400; Cellsafe, Korea) was used to synthesize cDNA from total RNA. qPCR amplification was detected using FastStart Universal SYBR Green Master reagent (04913914001; Roche, Switzerland) on a real-time PCR system. Gene expression levels were normalized to *ACTB*, and all samples were analyzed in triplicate. Supplementary Table 1 lists the primer sequences used in this study.

Site-directed mutagenesis and transfection

Site-directed mutagenesis of FLAG-LKB1 was conducted using the Phusion Flash High-Fidelity PCR master mix (F-548; Thermo Fisher Scientific, USA), following the manufacturer's instructions. TransIT-X2 (MIR6000; Mirus Bio, USA) was used to perform transient transfection.

In vitro translation

In vitro synthesis of protein complexes was performed using the TNT Quick Coupled Transcription/Translation System (L1170; Promega, UK), following the manufacturer's protocol. In brief, plasmid DNA constructs encoding human GCN5 and LKB1 under the control of the T7 promoter were used as templates for protein production. Each reaction contained 1.5 μg of plasmid DNA, 15 μL of TNT T7 Quick Master Mix, 1 μL of 1 mM Methionine, and 7.5 μL of nuclease-free water. Each reaction mix was incubated for 90 min at 30℃, and 20 μL of each reaction mixture was incubated with Flag M2 beads for the immunoprecipitation assay.

Small interfering RNAs (siRNAs)

All siRNAs were produced by GENOLUTION and transfected using RNAiMAX (13778150; Thermo Fisher Scientific, USA). The following siRNA sequences were used for GCN5 knockdown: for siGCN5 #1, sense 5′-GCCU CCAUUUGAGAAACCUAAUA-3′ and antisense 5′-UA UUAGGUUUCUCAAUGGAGGGC-3′; for siGCN5 #2, sense 5′-GAGAUCUAUGGGGCAAACUCUCC-3′ and antisense 5′-GGAGAGUUUGCCCCAUAGAUCUC-3′; for negative control, sense 5′-CCUCGUGCCGUUCCAU CAGGUAGUU-3′ and antisense 5′- CUACCUGAUGGA ACGGCACGAGGUU-3′.

Transwell migration assay

Cell migration was evaluated using Transwell chambers with 8 μm pore size polycarbonate membranes (37824, SPL, Korea), precoated with Matrigel. 24 h after transfection, 4×10^4 cells in 200 μL serum-free medium were seeded into the upper chamber. The lower chambers were filled with 800 μL serum-free medium with or without 20 ng/mL TGF-β to serve as a chemoattractant. After incubation at 37℃ for 24 h, cells that had migrated to the lower chamber were fixed with 4% paraformaldehyde for 5 min, permeabilized with 100% methanol for 20 min, and stained with 0.1% crystal violet for 30 min at room temperature. Non-migrating cells on the upper surface of the membrane were carefully removed with a cotton swab. Migrated cells were counted under a light microscope at ×200 magnification. The migration assay was performed in triplicate.

Wound healing assay

BEAS-2B cells were seeded into 6-well plates at a density of 2×10^5 cells/well and allowed to attach overnight. The cells were then transfected, and after 24 h, a linear scratch was created across the cell layer using a sterile 10 μL pipette tip. Detached cells were removed by gently washing with PBS, and the cells were subsequently cultured in complete medium with or without 20 ng/mL TGF-β for 24 h. Cell migration was quantified by measuring the distance migrated into the wound area using ImageJ software.

Hydroxyproline assay

Hydroxyproline content was quantified in mouse lung tissue (10 mg) using the hydroxyproline assay kit (BM-HYP-100; BIOMAX, Korea) following the manufacturer's protocol. Briefly, samples were homogenized, acid-hydrolyzed, neutralized, and then processed through the oxidation and chromogenic development steps of the kit. Absorbance was measured at 560 nm, and concentrations were calculated from a hydroxyproline standard curve.

Statistical analysis

All statistical analyses were performed using GraphPad Prism version 10 (GraphPad Software, USA). Data are presented as the mean ± standard deviation from at least three independent biological replicates. Comparisons between the two experimental groups were conducted using the Mann–Whitney test. One-way analysis of variance followed by Tukey's post hoc test was used for multiple comparisons. Statistical significance was denoted as $^{*}P < 0.05$, $^{**}P < 0.01$, $^{***}P < 0.001$, $^{****}P < 0.0001$. A P-value of < 0.05 was considered statistically significant.

Results

Expression of GCN5 is reduced in pulmonary fibrosis

To explore whether GCN5 expression is dysregulated in IPF, we first analyzed the publicly available transcriptomic dataset from the lung tissues of patients with IPF and healthy controls [52]. We revealed a significantly downregulated GCN5 in patients with IPF compared with the controls (Fig. 1A). Consistently, single-cell RNA sequencing data analysis from the integrated Human Lung Cell Atlas [53] further confirmed diminished GCN5 expression in the epithelial cells of IPF lungs (Fig. 1B).

To assess the clinical and pathophysiological relevance of GCN5 in IPF, we then investigated the expression levels of GCN5 in lung tissues from patients with IPF and two distinct pulmonary fibrosis mouse models. IHC analysis revealed a significantly reduced GCN5 protein level in the IPF lungs compared with the control samples (Fig. 1C). To further validate our observations in human samples, we assessed the expression levels of GCN5 in an inducible transgenic mouse model (*Ccsp-rtTA-tTs-TGF-β_1*), in which lung cell–specific DOX-induced TGF-β overexpression drives lung fibrosis (Figs. 1D and E), and in the lungs of BLM-treated mice (Figs. 1F and G). Both lung fibrosis models exhibited a significant decrease in GCN5 expression in fibrotic lung tissue.

We next examined the regional distribution of GCN5 by performing co-immunofluorescence (co-IF) staining using club cell secretory protein (CCSP) and surfactant protein C (SPC) as markers for bronchial and alveolar epithelial cells, respectively. In PBS-treated control lungs, GCN5 was preferentially expressed in the bronchial epithelium compared to the alveolar region. Following BLM administration, while GCN5 levels decreased in both compartments, the reduction was markedly more profound in CCSP-positive bronchial epithelial cells (Supplementary Fig. 1).

Consistent with these in vivo findings showing prominent downregulation in the bronchial epithelium, a reduction of GCN5 in lung epithelial cell lines, such as RLE-6TN (rat alveolar type II cells), C22 (mouse bronchial epithelial cells), and BEAS-2B (human bronchial epithelial cells), was also observed after treatment with the profibrotic mediator TGF-β (Supplementary Fig. 2A). Taken together, these findings indicate the downregulated GCN5 expression in pulmonary fibrosis and the potential role of GCN5 in fibrosis progression.

GCN5 suppresses EMT by promoting AMPK phosphorylation in lung epithelial cells

The EMT has been identified as a key pathological mechanism contributing to pulmonary fibrosis progression [11]. To investigate the role of GCN5 in regulating EMT in the context of lung fibrosis, we examined the expression of EMT markers in a lung fibrosis mouse model. Protein levels of GCN5 were significantly reduced in DOX-induced fibrotic lungs, along with a decrease in epithelial markers, such as E-cadherin and ZO-1, and an increase in mesenchymal markers, including N-cadherin and Vimentin (Fig. 2A). In agreement with previous studies indicating the anti-fibrotic role of phosphorylated AMPK [20, 21, 23], we observed a reduced AMPKα phosphorylation at threonine 172 (T172) in fibrotic lung tissues (Fig. 2A). To further validate these findings in vitro, bronchial epithelial cells were stimulated with TGF-β to induce EMT. Both GCN5 expression and AMPKα phosphorylation progressively decreased after TGF-β administration in C22 and BEAS-2B cells. (Fig. 2B and Supplementary Fig. 2B, respectively).

To identify the functional role of GCN5 in regulating EMT, we performed siRNA-mediated knockdown of GCN5 in BEAS-2B human bronchial epithelial cells. GCN5 silencing enhanced mesenchymal marker expression and significantly upregulated α-SMA, indicating a

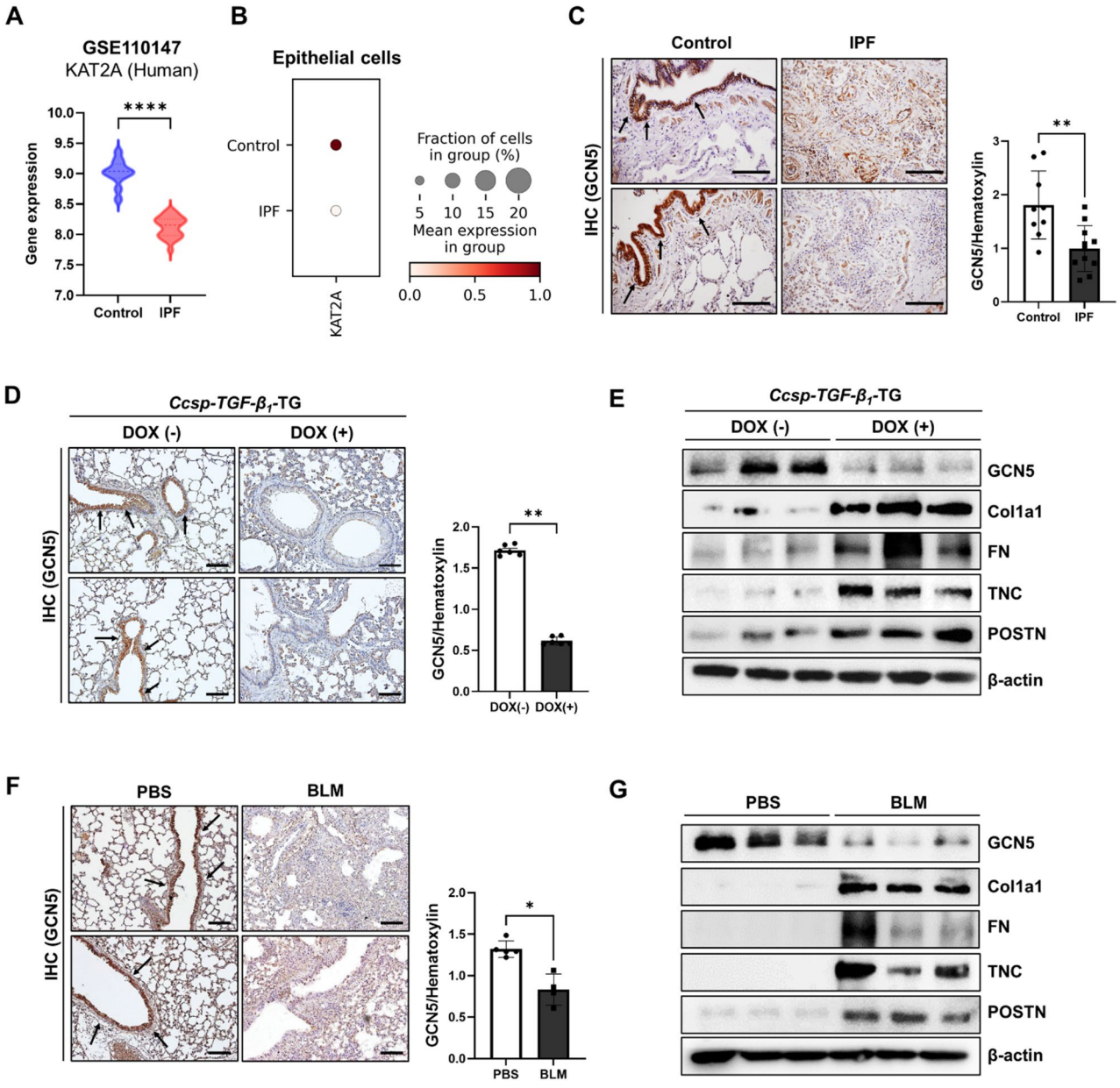

Fig. 1 GCN5 is downregulated in the fibrotic lungs of patients with IPF and mouse models. **A** mRNA levels of GCN5 (KAT2A) analyzed in patients with IPF (n = 22) and normal controls (n = 11) using the GSE110147 dataset. **B** Dot plot showing the mRNA expression of GCN5 (Ensembl ID: ENSG00000108773) in lung epithelial cells from patients with IPF and normal controls using single-cell RNA sequencing data from the integrated Human Lung Cell Atlas (HLCA). Only epithelial cells were selected for analysis based on cell-type annotations in the HLCA dataset [53]. **C** Representative images of GCN5 immunohistochemistry (IHC) in lung tissue sections from controls (n = 9) and patients with IPF (n = 11). Black arrows denote GCN5 expression in the bronchial epithelial region. Scale bars: 100 μm. The graph represents the GCN5 intensity normalized to hematoxylin from patients with IPF and controls. **D** Representative IHC images showing GCN5 expression in the lung samples from doxycycline (DOX)-treated Ccsp-rtTA-tTs-TGF-β1 transgenic and untreated control mice (n = 6 per group). Black arrows denote GCN5 expression in the bronchial epithelium. Scale bars: 50 μm. The graph illustrates the GCN5 intensity normalized to hematoxylin from control and transforming growth factor-beta (TGF-β)-overexpressed mice. **E** Immunoblotting analysis performed using the indicated antibodies in lung tissues from the transgenic mice. **F** Representative IHC images of GCN5 expression in lung tissues from mice intratracheally injected with 2 mg/kg of bleomycin (BLM) or phosphate-buffered saline (PBS) (n = 5 per group). Black arrows denote GCN5 localization in the bronchial epithelial area. Scale bars: 50 μm. The graph represents the GCN5 intensity/hematoxylin ratio from PBS- and BLM-treated mice. **G** Immunoblotting analysis performed using the indicated antibodies in the lung tissues from the control and BLM-treated mice. Data are presented as mean ± SEM, $^{*}P < 0.05$, $^{**}P < 0.01$, and $^{****}P < 0.0001$ by two-tailed Mann–Whitney test for two groups

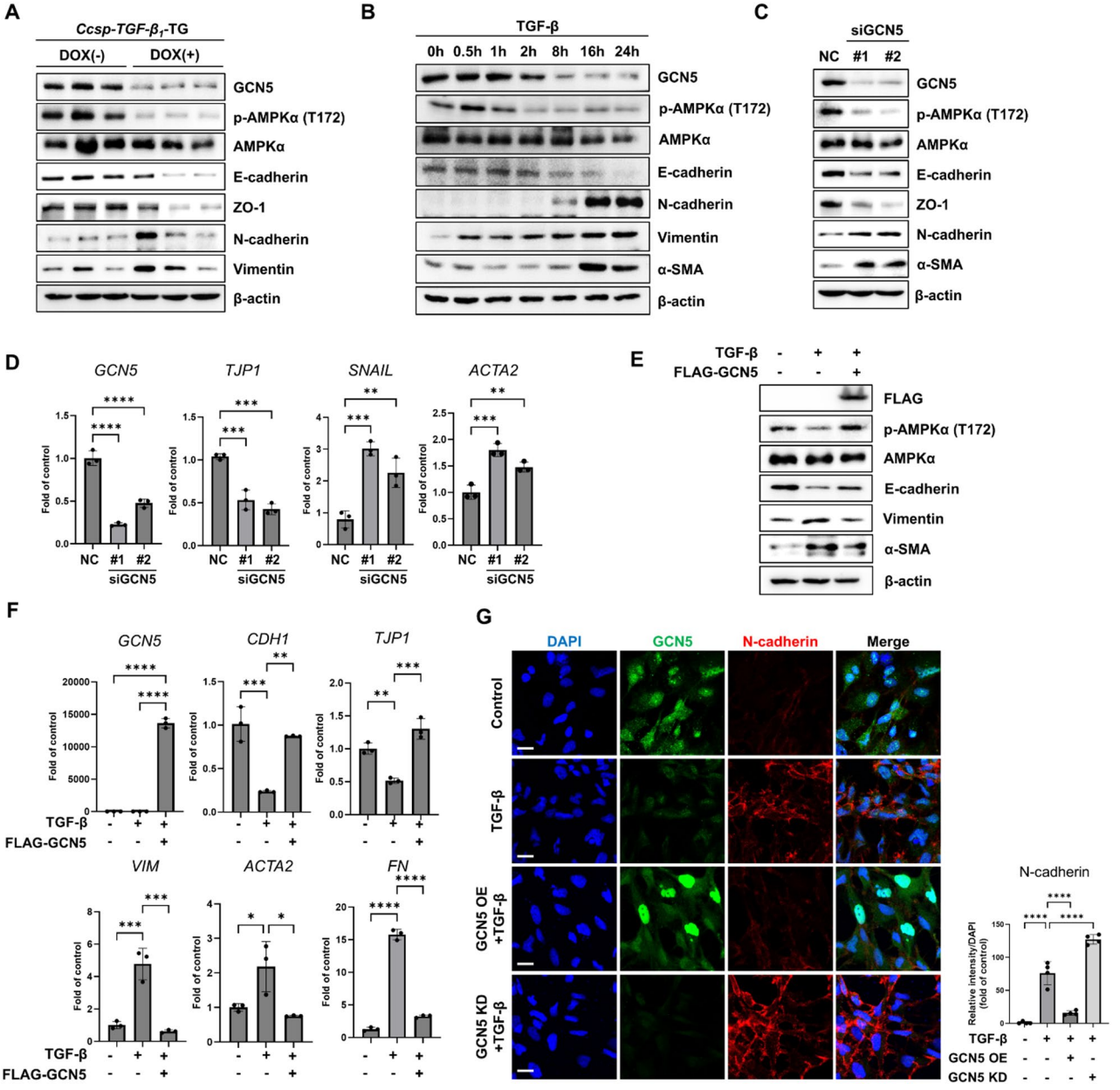

Fig. 2 GCN5 suppresses EMT by maintaining AMPK signaling in bronchial epithelial cells. **A** Western blot analysis showing the protein levels of GCN5, phospho-AMPKα, and epithelial-to-mesenchymal transition (EMT)-related markers in lung tissues from DOX-untreated control and DOX-treated TGF-β–overexpressing transgenic mice (n = 3 per group). **B** Western blot analysis representing time-dependent changes in GCN5, phospho-AMPKα, and EMT-related proteins in C22 bronchial epithelial cells. Cells were treated with 20 ng/mL TGF-β and harvested at the indicated time points. **C**, **D** (**C**) Western blot analysis of protein expression and (**D**) qRT-PCR analysis of mRNA levels for GCN5 and EMT-related markers in BEAS-2B cells after GCN5 knockdown. The cells were transfected with 20 nM of GCN5-specific siRNAs or control siRNA. After 48 h, cells were collected for analysis. **E**, **F** (**E**) Immunoblot analysis of protein expression and (**F**) qRT-PCR analysis of mRNA levels for GCN5 and EMT-associated markers in BEAS-2B cells after GCN5 overexpression with TGF-β treatment. Cells were transfected with 2 μg of either empty vector or FLAG-tagged GCN5 plasmid. After 24 h, the cells were treated with 20 ng/mL of TGF-β for an additional 24 h. **G** Representative immunocytochemistry (ICC) images showing N-cadherin expression in BEAS-2B cells after a 20 ng/mL TGF-β treatment for 24 h, with GCN5 overexpression or knockdown. Scale bars: 10 μm. Data are presented as mean ± SEM, $^{*}P < 0.05$, $^{**}P < 0.01$, $^{***}P < 0.001$, and $^{****}P < 0.0001$ by ordinary one-way analysis of variance (ANOVA) for multiple groups

phenotypic shift toward fibroblast-like characteristics (Figs. 2C and D). We observed that GCN5 knockdown in BEAS-2B cells induced a morphological transition toward a more elongated, spindle-shaped phenotype, indicating mesenchymal characteristics (Supplementary Fig. 3A). Further, the increase in N-cadherin expression observed upon GCN5 knockdown was attenuated with AMPK activator Metformin treatment, as shown by

ICC (Supplementary Fig. 3B). Consistently, Metformin administration restored E-cadherin expression in GCN5-silenced cells (Supplementary Fig. 3C).

Conversely, GCN5 overexpression restored AMPK phosphorylation and epithelial markers, such as *CDH1* (E-cadherin) and *TJP1* (ZO-1), while suppressing mesenchymal and fibrotic markers including *VIM* (Vimentin), *ACTA2* (α-SMA), and *FN* (Fibronectin) (Figs. 2E and F), supporting the hypothesis that GCN5 modulates EMT through AMPK signaling. Consistent with these findings, ectopic expression of GCN5 suppressed N-cadherin and Col1a1 induction in response to TGF-β stimulation, whereas GCN5 knockdown further increased mesenchymal marker gene expression (Fig. 2G and Supplementary Fig. 3D). Consequently, we confirmed that these molecular alterations led to phenotypic changes. Wound healing and Transwell assays revealed that GCN5 overexpression effectively attenuated TGF-β-induced cell motility and migration, whereas GCN5 knockdown exacerbated these migratory phenotypes (Supplementary Fig. 4).

In contrast to the findings in epithelial cells, we observed distinct responses in lung fibroblasts. We performed parallel loss- and gain-of-function studies in human lung fibroblasts (MRC-5) to address cell type specificity. GCN5 knockdown in fibroblasts did not alter AMPK phosphorylation or the expression of fibroblast activation markers including Col1a1, α-SMA, and FN. Furthermore, GCN5 overexpression failed to rescue AMPK phosphorylation or suppress the TGF-β-induced upregulation of profibrotic markers (Supplementary Fig. 5).

These results indicate that GCN5 suppresses the EMT of lung epithelial cells by maintaining AMPK activation.

GCN5 directly binds to LKB1, and the interaction is disrupted in pulmonary fibrosis

AMPK phosphorylation is mediated by LKB1, a well-established upstream kinase of AMPK, and LKB1 is known to regulate EMT and pulmonary fibrosis [28, 29]. Although N-terminal deacetylation at lysine 48 (K48) of LKB1 by SIRT1 has been previously reported [34, 54], the specific lysine acetyltransferase (KAT) responsible for LKB1 acetylation remains unknown in the context of fibrosis. Based on this evidence, we hypothesized that GCN5 regulates AMPK phosphorylation through LKB1.

To assess the interaction between GCN5 and LKB1, we use an in silico molecular docking and visualization system. The structure of the chimeric protein was generated using homology modeling. The FASTA sequence was submitted to AlphaFold 3, an online server for 3D protein structure prediction, to obtain the most accurate and stable configuration of the fusion construct. AlphaFold 3 predicts the 3D protein structure based only on the primary amino acid sequence with high accuracy of the side chains. Among the predicted models, the top-ranked AlphaFold 3 structure was selected and proceeded for further analysis. To identify the mechanism of the interaction between GCN5 (uniprot: Q92830) and LKB1 (uniprot: Q15831), HADDOCK protein–protein docking was performed. The top structure based on the score, electrostatic energies, and Van der Waals attraction was selected for interaction studies. Among protein–protein docking, the major interactions are electrostatic and Van der Waals, which mutually find accurate results along with promising levels as a scoring function. The HADDOCK server clustered 200 structures, and the analysis revealed that K403, K416, K423, and K431 residues of LKB1 were involved in complex formation with GCN5 (Fig. 3A, middle panel). Lysine residues are known to participate in various posttranslational modifications, including acetylation, ubiquitination, and methylation [55, 56]. Considering the role of GCN5 as a KAT [57, 58], it is plausible that this interaction could lead to the acetylation of LKB1, or that the interaction itself is regulated by the acetylation status of these lysine residues. Red dashed lines within the right panel represent hydrogen bonds, indicating that specific residue-level contacts contribute to the stability of the GCN5-LKB1 complex (right panel).

To confirm the direct binding of GCN5 and LKB1, we performed immunoprecipitation using in vitro translated proteins. We observed a direct interaction between GCN5 and LKB1, indicating the possibility that GCN5 directly acetylates LKB1 (Fig. 3B). We then tested the changes in this association in TGF-β–treated BEAS-2B cells and fibrotic tissues. Immunoprecipitation analysis revealed a decreased GCN5 expression and a reduced binding of GCN5 and LKB1 upon TGF-β treatment (Fig. 3C). To further confirm this interaction, we examined the intracellular distribution of GCN5 and LKB1 in BEAS-2B cells and observed clear co-localization of both proteins within the cytoplasm (Supplementary Fig. 6). This finding provides evidence that GCN5 is spatially positioned to regulate LKB1 in the cytosolic compartment, where AMPK signaling is predominantly active.

We next examined the relevance of the GCN5–LKB1 interaction using two lung fibrosis mouse models. Compared with the control tissues, both the BLM-induced mouse model and the TGF-β–overexpressing transgenic model demonstrated reduced GCN5 and LKB1 expression, along with decreased co-localization of the two proteins (Figs. 3D and E). These findings indicate the interaction between GCN5 and LKB1 under normal physiological conditions, but this interaction is disrupted in the fibrotic lung microenvironment.

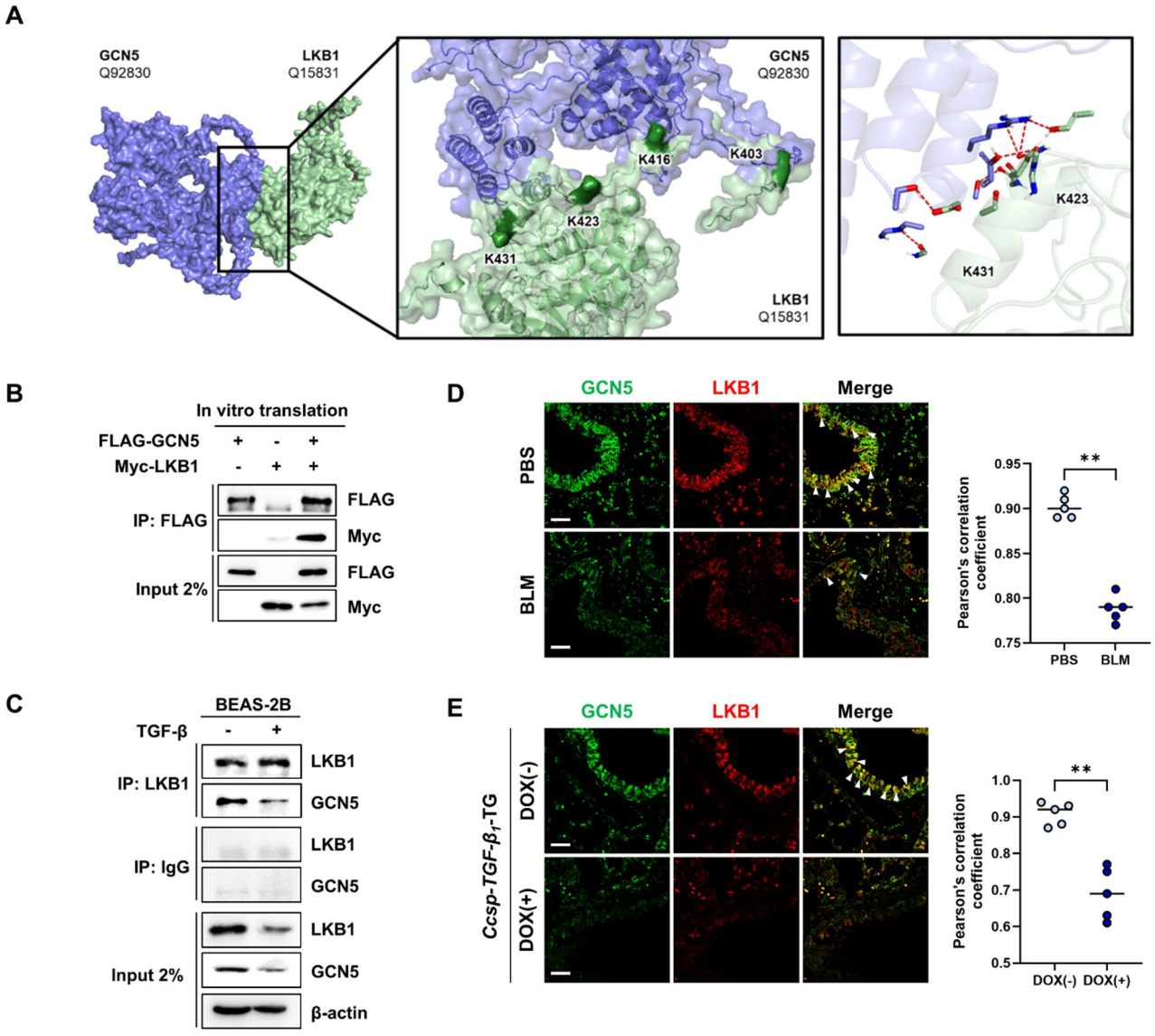

Fig. 3 GCN5 directly binds to LKB1, and their interaction is reduced under fibrotic conditions. **A** Structural basis of the LKB1–GCN5 interaction. (Left) Surface representation of the LKB1 (palegreen) and GCN5 (slate) complex, demonstrating their direct physical association. The black box denotes the region magnified in the middle panel (middle). Magnified view highlighting key lysine residues (LKB1: K403, K416, K423, and K431) shown in green surface representation. (Right) Detailed atomic view of the interface, emphasizing specific residue-level interactions. Red dashed lines indicate potential hydrogen bonds mediating the stability of the complex. **B** In vitro binding assay of FLAG-tagged GCN5 and Myc-tagged LKB1. FLAG-GCN5 and Myc-LKB1 were translated in vitro and immunoprecipitated using Flag M2 beads. Co-precipitated LKB1 was detected using anti-Myc immunoblotting. **C** Co-immunoprecipitation of endogenous GCN5 with LKB1 in BEAS-2B cells treated with 20 ng/mL of TGF-β for 24 h. Cell lysates were immunoprecipitated with an anti-LKB1 antibody or control IgG, followed by immunoblotting for GCN5 and LKB1. **D**, **E** Representative immunofluorescence (IF) images showing the downregulated protein expression of GCN5 and LKB1 as well as decreased co-localization in (**D**) BLM-treated or (**E**) TGF-β-transgenic mice (n = 5 per group). White arrowheads denote the co-localization of GCN5 and LKB1. Scale bars: 20 μm. The scatter plots illustrate the correlation between GCN5 and LKB1 fluorescence intensity, as analyzed using the Coloc 2 plugin in ImageJ. Pearson's correlation coefficient was calculated to quantitatively assess the degree of colocalization. Data are presented as mean ± SEM, $^{**}P < 0.01$ using a two-tailed Mann–Whitney test for two groups

GCN5 regulates LKB1–AMPK signaling via LKB1 acetylation at K431

GCN5 is a well-characterized KAT that regulates the function of its substrates by changing their acetylation status [41, 59]. We aimed to systematically determine the lysine residues targeted by GCN5, because the acetylation sites on LKB1 regulated by GCN5 have not been studied. In silico docking analysis revealed that GCN5 is likely to bind the C-terminal lysine residues of LKB1 (K403, K416, K423, and K431). Based on this prediction, we reviewed a previous study that identified acetylation sites on LKB1 using MALDI-TOF and LC-MS/MS [34]. Mass spectrometric profiling identified at least nine acetylated lysines, including the C-terminal residues K416, K423, and K431,

which are evolutionarily conserved across humans, mice, and rats (Fig. 4A). Moreover, GCN5-mediated LKB1 acetylation was validated by an in vitro acetylation assay (Fig. 4B).

To investigate the role of GCN5-mediated acetylation in regulating LKB1 function, we performed site-directed mutagenesis by substituting K403, K416, K423, and K431 with glutamine residues (K403Q, K416Q, K423Q, and K431Q). Glutamine substitution mimics acetylated lysine by providing a polar, uncharged residue. LKB1 phosphorylation at Ser428 (a human ortholog of mouse Ser431) is considered a functional marker of LKB1 activation [60]. To assess the association of these acetyl-mimetic replacements with LKB1 activity, LKB1 was co-expressed with its cofactors STRAD and MO25 [61] in BEAS-2B cells. Among the single mutants, K431Q significantly improved LKB1 phosphorylation (Fig. 4C). In parallel with these results, we observed an increase in AMPK

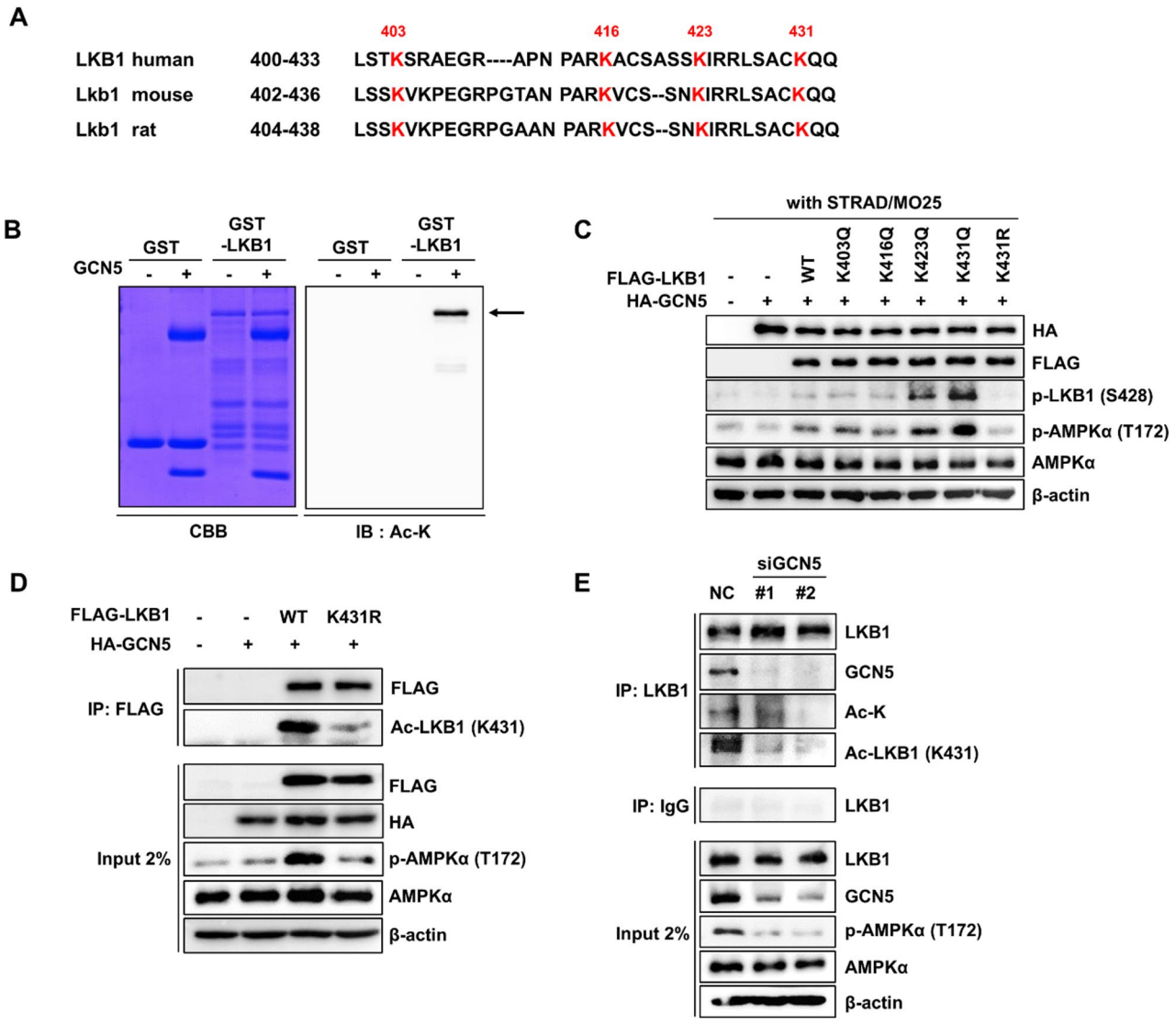

Fig. 4 GCN5 acetylates LKB1 at multiple lysine residues, with K431 as a key regulatory site. **A** Alignment of the C-terminal amino acid sequences of LKB1 from human (residues 400–433), mouse (402–436), rat (404–438), with conserved lysine residues (K403, K416, K423, and K431 in human) highlighted in red. The structural modeling of the LKB1–GCN5 complex indicates the involvement of these residues in complex formation. **B** In vitro acetylation of LKB1 by GCN5. (Right) Purified GST or GST–LKB1 was incubated with recombinant human GCN5 and analyzed by immunoblotting for anti-Acetylated-Lysine (Ac-K). The black arrow indicates acetylated LKB1. (Left) Coomassie Brilliant Blue (CBB) staining confirms equal loading of the GST fusion proteins. **C** BEAS-2B cells were co-transfected with GCN5 and LKB1 acetyl-mimetic single mutants (K403Q, K416Q, K423Q, and K431Q), or the deacetylation-mimetic mutant K431R in the presence of STRAD/MO25. After 48 h, the cell lysates were analyzed by immunoblotting with the indicated antibodies. **D** LKB1 immunoprecipitation in BEAS-2B cells transfected with either WT or K431R mutant. Acetylation at K431 was detected using an acetylation site–specific antibody. The cells were collected and analyzed by western blotting using the indicated antibodies 48 h post-transfection. **E** Immunoprecipitation of endogenous LKB1 in BEAS-2B cells with GCN5 knockdown. Cells were treated with 20 nM of siRNAs for 48 h. Acetylation was analyzed using a pan-acetyl-lysine antibody and a specific antibody recognizing LKB1 acetylation at K431

phosphorylation. These data confirmed that acetylation at LKB1 K431 plays a crucial role in regulating LKB1 activity.

To further examine the functional significance of K431 acetylation, we generated a K431 mutant in which lysine was substituted with arginine (K431R). This substitution mimics the unacetylated state while preserving the positive charge. Importantly, we developed an antibody specifically recognizing acetylated LKB1 at lysine 431 (Ac-LKB1 K431) to assess K431 mutation–induced acetylation changes. BEAS-2B cells were co-transfected with GCN5 and either LKB1 wild-type (WT) or the K431R mutant. Immunoprecipitation analysis revealed the reduced GCN5-mediated acetylation at K431 in the K431R mutant, along with decreased AMPK phosphorylation (Fig. 4D), thereby validating the functional role of GCN5-mediated K431 acetylation on LKB1 function. Finally, we investigated whether endogenous GCN5 regulates LKB1 acetylation and its functional activity. GCN5 knockdown using siRNA reduced the total LKB1 acetylation, accompanied by decreased K431-specific acetylation and AMPK phosphorylation (Fig. 4E). To confirm the clinical relevance of these findings, we further examined the relationship between GCN5 and LKB1 acetylation in human lung tissues. Using the specific antibody against acetylated LKB1 at K431, we performed co-IF staining on lung sections from control donors and patients with IPF. Consistent with our in vitro data, LKB1 K431 acetylation and GCN5 signals were both significantly reduced in the fibrotic lesions of IPF lungs. (Supplementary Fig. 7).

Taken together, these results reveal that the GCN5-mediated LKB1 acetylation increases LKB1 activity and subsequent AMPK pathway activation, and substantiates the clinical relevance of this signaling axis in IPF.

GCN5 overexpression attenuates lung fibrosis in the BLM-induced mouse model

Considering our results indicating that GCN5 suppresses key fibrotic processes in the lung, we then explored whether GCN5 overexpression could alleviate fibrosis progression in vivo. To achieve targeted expression of GCN5 in the lung, we generated a serotype 5 adenoviral vector encoding HA-tagged GCN5 (Ad5-GCN5-HA). HA-tagged GCN5 overexpression after adenoviral infection was confirmed in BEAS-2B cells using fluorescence microscopy and western blotting (Supplementary Fig. 8).

Eight-week-old male mice received intratracheal instillation of either BLM or saline (PBS) in combination with Ad5-GCN5-HA. The mice were sacrificed at 8 days post administration, and the lung tissue samples were collected for histological and molecular analyses (Fig. 5A). Masson's trichrome staining and hydroxyproline assay demonstrated that GCN5 overexpression significantly suppressed fibrosis progression, as evidenced by a reduction in collagen deposition. IHC analysis further confirmed the decreased α-SMA expression in the GCN5-overexpressing group treated with BLM (Figs. 5B-D). BAL fluid cell counts reflect immune cell infiltration in response to lung injury. GCN5 overexpression significantly reduced total BAL cell counts in BLM-treated mice compared with those receiving the empty Ad5 vector (Supplementary Fig. 9A). Adenovirus-mediated GCN5 expression decreased fibrotic marker expression, such as Col1a1 and Tenascin C (TNC), indicating reduced myofibroblast activation. Conversely, the reduction of E-cadherin, AMPK phosphorylation, and LKB1 acetylation at K431 induced by BLM treatment was reversed by GCN5 overexpression (Fig. 5E). Furthermore, GCN5 overexpression suppressed fibrotic and EMT-associated gene expression in the BLM-induced model (Fig. 5F). To specifically assess EMT in the airway epithelium, we performed co-IF staining for N-cadherin and the bronchial epithelial marker CCSP. The BLM-induced upregulation of N-cadherin within CCSP-positive bronchial epithelial cells was significantly attenuated by GCN5 overexpression (Fig. 5G). Consistently, IF staining of Col1a1 revealed that GCN5 overexpression alleviated BLM-induced fibrosis. Furthermore, ZO-1 expression, which was markedly decreased after BLM treatment, was restored upon GCN5 overexpression (Supplementary Figs. 9B and C). Collectively, these findings indicate that GCN5 negatively regulates pulmonary fibrosis by suppressing myofibroblast activation, restoring epithelial characteristics, and inhibiting EMT through LKB1 acetylation at K431.

Discussion

The exact pathogenesis of pulmonary fibrosis remains unclear due to the complex factors that contribute to lung tissue remodeling despite extensive research on the molecular mechanisms underlying pulmonary fibrosis, including IPF. Repeated microinjuries to the aged lung epithelium, dysregulated wound healing, and excessive ECM deposition play a crucial role in IPF pathogenesis. Excessive accumulation of ECM components, including hyaluronic acid, fibronectin, proteoglycans, and interstitial collagens, contributes to fibrogenesis by promoting uncontrolled wound healing in myofibroblasts [62]. The origin of myofibroblasts that drive IPF remains unclear and is still widely discussed. However, several mechanisms underlying IPF pathogenesis have been suggested, including the proliferation and differentiation of resident lung fibroblasts, the transition of bone marrow–derived fibrocytes or circulating progenitors into fibroblasts, and EMT [63]. Although the precise role of EMT in IPF remains controversial, increasing evidence suggests that it may contribute to the abnormal epithelial-fibroblast crosstalk that promotes fibrosis [64]. Progressive fibrotic remodeling in IPF is increasingly understood to arise

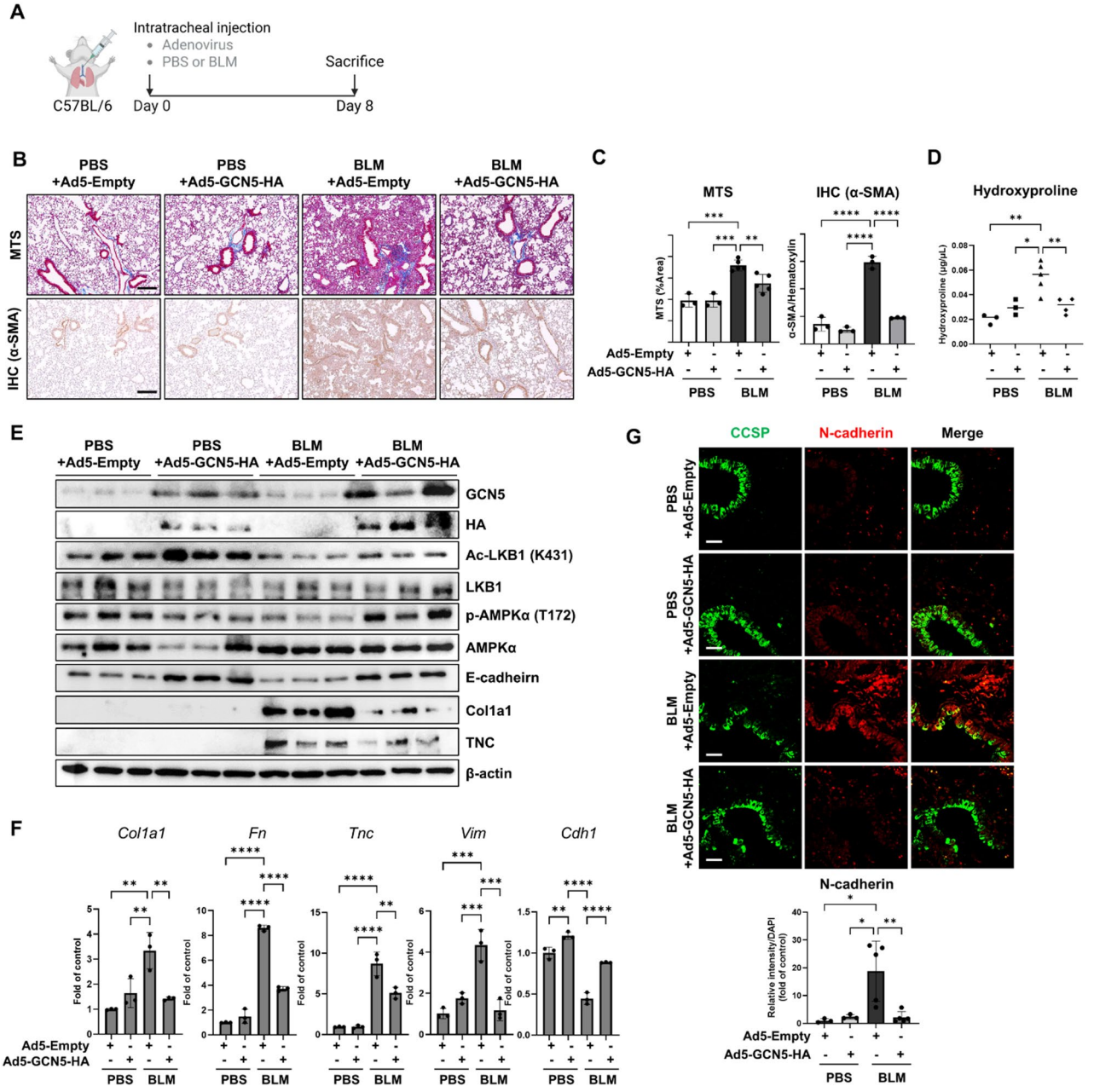

Fig. 5 Overexpression of GCN5 attenuates fibrosis in the BLM-induced mouse model. **A** Schematic representation illustrating the experimental design. C57BL/6 mice were intratracheally injected with 2 mg/kg BLM or PBS together with adenovirus (2.0 × 1011 VP) carrying either GCN5 or an empty control. The mice were sacrificed 8 days after injection. The numbers per group are: PBS + Ad5-Empty (n = 3), PBS + Ad5-GCN5-HA (n = 3), BLM + Ad5-Empty (n = 5), and BLM + Ad5-GCN5-HA (n = 5). **B** Representative images of Masson's trichrome staining (MTS) and IHC analysis of α-SMA in lung sections from mice treated with PBS or BLM with or without GCN5 overexpression. Scale bars: 50 μm. **C** Quantification of the fibrotic area (MTS) (left) and α-SMA-positive DAB area normalized to hematoxylin (right). **D** Total cell counts in BAL fluid were determined after BLM or PBS instillation in adenovirus-instilled mice. **E**, **F** (**E**) Protein expression and (**F**) mRNA levels of fibrosis and EMT markers in lung tissues of PBS- or BLM-treated mice transduced with Ad5-Empty or Ad5-GCN5-HA (n = 3 per group). **G** Representative IF images showing N-cadherin expression within CCSP-positive bronchial epithelium in lung sections from each group. Scale bars: 20 μm. The graph represents the quantification of the N-cadherin signal intensity normalized to DAPI. Data are presented as mean ± SEM, *$P < 0.05$, **$P < 0.01$, ***$P < 0.001$, and ****$P < 0.0001$ by ordinary one-way ANOVA for multiple groups

from EMT-like reprogramming of genetically vulnerable bronchoalveolar epithelium, which promotes bronchiolization, aberrant epithelial-mesenchymal crosstalk, and sustained fibrotic progression rather than effective alveolar regeneration [65]. In this study, we revealed a novel regulatory mechanism by which GCN5 maintains LKB1 acetylation and downstream AMPK activation, thereby suppressing EMT and fibrotic progression

of epithelial cells. Although the reduction of GCN5 is most prominent in airway epithelial regions, its loss may nonetheless contribute indirectly to fibrotic remodeling by promoting epithelial plasticity, bronchiolization, and metaplasia, thereby amplifying maladaptive epithelial-mesenchymal crosstalk. Collectively, our findings establish GCN5 as a critical regulator of lung epithelial homeostasis and highlight disruption of the GCN5–LKB1–AMPK axis as a key contributor to the pathogenesis of pulmonary fibrosis.

A recent study demonstrated that LKB1 inactivation in alveolar type II (ATII) epithelial cells inhibits autophagy and induces EMT [28]. LKB1 depletion promotes fibrotic progression through the loss of CAB39L, a regulatory subunit of MO25, which is crucial for LKB1 activation. EMT induction in fibrosis has been associated with autophagy inhibition through the p62/SQSTM1-NFκB-Snail2 signaling pathway [11, 66]. LKB1 is a serine/threonine kinase that functions as an upstream activator of AMPK, which is a key regulator of cellular energy homeostasis, growth, and metabolism. LKB1 exhibits a protective role in fibrosis by inhibiting myofibroblast differentiation. LKB1–AMPK pathway disruption is implicated in various fibrotic diseases, including liver, kidney, and lung fibrosis [28, 67, 68]. Dysregulation of the LKB1–AMPK signaling pathway contributes to ECM accumulation by impairing autophagy and disrupting cellular energy metabolism. Several therapeutic strategies that target the LKB1–AMPK pathway have been proposed for fibrotic diseases [69, 70], although the regulatory mechanisms underlying this pathway in fibrosis have yet to be fully elucidated. LKB1 itself is a constitutively active kinase, but its activity is regulated through phosphorylation at multiple sites, including Ser31/307/325/428 and Thr185/189/336/366 [60]. The phosphorylation status of LKB1 influences its interaction with STRAD/MO25 and affects downstream signaling pathways. A study on LKB1 deacetylation by SIRT1 at K48 in HEK293 cells [34] revealed that the deacetylation modulates its intracellular localization and AMPK activation; however, its association with disease progression remains unclear. In this study, we identified K431 acetylation by GCN5 as a key regulatory mechanism of LKB1 in pulmonary fibrosis. We observed that GCN5 overexpression reversed the reduction of LKB1 acetylation and phosphorylation by BLM-induced lung fibrosis, which consequently increased AMPK phosphorylation and suppressed EMT. Further studies using lung epithelial cell–specific GCN5 knockout mice could clarify the anti-pulmonary fibrotic function of GCN5, which mediates LKB1 acetylation and AMPK phosphorylation.

Dysregulation of epigenetic control causes imbalances in cellular homeostasis, resulting in various diseases. HATs, which are representative enzyme proteins of epigenetic regulation, have also been associated with the induction of fibrotic diseases. We recently reported that increased p300 protein stability in ATII cells, mediated by the deubiquitinase UCHL3, promotes lung fibrosis [46]. In addition, we demonstrated that increased p300 expression in proximal tubular epithelial cells improves renal fibrosis through partial endothelial-to-mesenchymal transition [71]. Furthermore, the liver stiffness–induced stabilization of p300 promotes the differentiation of hepatic stellate cells into myofibroblasts [72]. In contrast, loss of PCAF in proximal tubular cells induces renal fibrosis, regulating adherens junction-related genes [73]. Emerging evidence has implicated GCN5 in the pathogenesis of various diseases, including cancer, cardiovascular disease, and metabolic dysfunction [40]. It has been regulated by both the lysosomal degradation pathway in vascular smooth muscle cell migration [74] and the ubiquitin–proteasome system via the Cul4a-Dbd1 E3 ligase complex in mouse embryonic fibroblasts [75]. Notably, in this study, GCN5 protein levels were markedly reduced in TGF-β–treated epithelial cells as well as in fibrotic mouse lung tissues, indicating a potential association between GCN5 downregulation and fibrotic remodeling. The specific upstream regulators that mediate GCN5 degradation or suppression under fibrotic conditions remain unknown; nevertheless, these findings raise the possibility that post-translational regulation of GCN5 is a key node in fibrogenic signaling. Future studies are recommended to focus on identifying the molecular pathways responsible for GCN5 turnover and determining whether modulating GCN5 stability or activity can reverse fibrotic phenotypes in vivo.

Furthermore, considering the transient expression profile of the adenoviral vector used in this study, our in vivo assessment was confined to early phases of fibrotic progression/EMT. While these findings confirm the protective effect of GCN5 during the initiation of fibrosis, evaluating its efficacy in established fibrosis necessitates sustained expression. Future work will therefore employ Adeno-associated virus (AAV) vectors to test the long-term durability of GCN5 restoration. In addition, utilizing AAV vectors with airway epithelial cell-specific promoters will enable precise compartment-targeted expression, thereby validating the therapeutic potential of targeting the GCN5-LKB1 axis in specific lung lineages.

Overall, we identify GCN5 as a novel anti-fibrotic regulator that preserves lung epithelial homeostasis by acetylating LKB1 at K431 to activate AMPK and suppress EMT. Together, our findings reveal the GCN5–LKB1–AMPK axis as a key molecular pathway disrupted in IPF and a promising therapeutic target for attenuating fibrotic progression.

Conclusions

Taken together, this study provides new insights into the regulatory role of GCN5 in pulmonary fibrosis. We revealed that the loss of GCN5 modulates pulmonary fibrosis by suppressing LKB1–AMPK signaling, which subsequently induces EMT. Therefore, we propose that GCN5 may serve as a novel therapeutic target for the diagnosis and treatment of pulmonary fibrosis.

Abbreviations

IPF	Idiopathic pulmonary fibrosis
ECM	Extracellular matrix
GCN5	General control non-depressible 5
AMPK	AMP-activated protein kinase
LKB1	Liver kinase B1
EMT	Epithelial-to-mesenchymal transition
TGF-β	Transforming growth factor-beta
HAT	Histone acetyltransferase
KAT	Lysine acetyltransferase
BLM	Bleomycin
DOX	Doxycycline
BAL	Bronchoalveolar lavage
FBS	Fetal bovine serum
DMEM	Dulbecco's Modified Eagle's Medium
PBS	Phosphate-buffered saline
EDTA	Ethylenediaminetetraacetic acid
PBST	PBS containing Tween-20
HRP	Horseradish peroxidase
3D	Three-dimensional
IHC	Immunohistochemistry
DAB	3,3′-Diaminobenzidine
IF	Immunofluorescence
DAPI	4′,6-diamidino-2-phenylindole
ICC	Immunocytochemistry
qRT-PCR	Quantitative reverse transcription-polymerization chain reaction
ATII	Alveolar type II

Supplementary Information

The online version contains supplementary material available at https://doi.org/10.1186/s12964-026-02757-8.

Supplementary Material 1.

Supplementary Material 2.

Acknowledgements

Not applicable.

Authors' contributions

S.B. and S.Y.P. conceived and designed the experimental approach, performed the experiments, and prepared the manuscript. H.K., S.H.L., J.H.K., H.K., and J.Y.Y. prepared the materials and analyzed the results. M.H.S., H.S.S., and M.S.P. provided the human IPF lung samples and support for the clinical interpretation of the data. C.G.L. conceived the experimental approach and provided support for the analysis of the data. J.A.E. provided support for the TGF-β 1 -TG lung fibrosis mouse model. H.G.Y. conceived and designed the experimental approach, performed data analysis, and prepared the manuscript. All authors contributed to the final version of the manuscript.

Funding

This research was supported by the National Research Foundation of Korea (NRF) MRC grant funded by the Korean government (MSIT) (No. RS-2025-02214844), the National Research Foundation of Korea (NRF) grants funded by the Korean government (MOE) (No. RS-2025-25397284 to S.Y.P.), Basic Science Research Program through the NRF funded by the Ministry of Education (No. RS-2025-25438750 to H.K), and the grant of the Korea Health Technology R&D Project through the Korea Health Industry Development Institute (KHIDI), funded by the Ministry of Health & Welfare, Republic of Korea (RS-2025-02214298).

Data availability

The datasets analyzed during the current study are publicly available from the Gene Expression Omnibus (GEO) under accession number GSE110147 (https://www.ncbi.nlm.nih.gov/geo/query/acc.cgi?acc=GSE110147) [52] and from CELLxGENE portal (https://cellxgene.cziscience.com/collections/6f6d381a-7701-4781-935c-db10d30de293) [53].

Declarations

Ethics approval and consent to participate

The Ethics Committee of the Institutional Review Board of Severance Hospital (protocol no. 4-2019-0447) approved this study. All patients signed written consent. All animal experiments were approved by the Institutional Animal Care and Use Committee of Yonsei University College of Medicine (IACUC No. 2023-0025).

Consent for publication

Not applicable.

Competing interests

The authors declare no competing interests.

Author details

[1]Department of Biochemistry and Molecular Biology, Graduate School of Medical Science, Brain Korea 21 Project, Yonsei University College of Medicine, Seoul 120-752, Korea
[2]Department of Pediatrics and Institute of Allergy, Severance Medical Research Institute, Yonsei University College of Medicine, Seoul, Korea
[3]Department of Pathology, Yonsei University College of Medicine, Seoul, Korea
[4]Division of Pulmonary and Critical Care Medicine, Department of Internal Medicine, Yonsei University College of Medicine, Seoul, Korea
[5]Hanyang University, Intercollege, Seoul, Korea
[6]Department of Molecular Biology, Cell Biology and Biochemistry, Brown University, Providence, RI, USA
[7]Department of Biomedical Laboratory Science, Yonsei University MIRAE Campus, Wonju, Korea

Received: 3 September 2025 / Accepted: 20 February 2026
Published online: 20 April 2026

References

1. Lederer DJ, Martinez FJ. Idiopathic Pulmonary Fibrosis. N Engl J Med. 2018;378(19):1811–23.
2. Raghu G, Remy-Jardin M, Richeldi L, Thomson CC, Inoue Y, Johkoh T, et al. Idiopathic Pulmonary Fibrosis (an Update) and Progressive Pulmonary Fibrosis in Adults: An Official ATS/ERS/JRS/ALAT Clinical Practice Guideline. Am J Respir Crit Care Med. 2022;205(9):e18–47.
3. Martinez FJ, Collard HR, Pardo A, Raghu G, Richeldi L, Selman M, et al. Idiopathic pulmonary fibrosis. Nat Rev Dis Primers. 2017;3:17074.
4. Mei Q, Liu Z, Zuo H, Yang Z, Qu J. Idiopathic Pulmonary Fibrosis: An Update on Pathogenesis. Front Pharmacol. 2021;12:797292.
5. Heukels P, Moor CC, von der Thusen JH, Wijsenbeek MS, Kool M. Inflammation and immunity in IPF pathogenesis and treatment. Respir Med. 2019;147:79–91.
6. King TE Jr., Pardo A, Selman M. Idiopathic pulmonary fibrosis. Lancet. 2011;378(9807):1949–61.
7. Rout-Pitt N, Farrow N, Parsons D, Donnelley M. Epithelial mesenchymal transition (EMT): a universal process in lung diseases with implications for cystic fibrosis pathophysiology. Respir Res. 2018;19(1):136.
8. Youssef KK, Nieto MA. Epithelial-mesenchymal transition in tissue repair and degeneration. Nat Rev Mol Cell Biol. 2024;25(9):720–39.
9. Mottais A, Riberi L, Falco A, Soccal S, De Gohy S. Rose V. Epithelial-Mesenchymal Transition Mechanisms in Chronic Airway Diseases: A Common Process to Target? Int J Mol Sci. 2023;24(15):12412.

10. Jin H, Park SY, Lee JE, Park H, Jeong M, Lee H, et al. GTSE1-driven ZEB1 stabilization promotes pulmonary fibrosis through the epithelial-to-mesenchymal transition. Mol Ther. 2024;32(11):4138–57.
11. Hill C, Jones MG, Davies DE, Wang Y. Epithelial-mesenchymal transition contributes to pulmonary fibrosis via aberrant epithelial/fibroblastic cross-talk. J Lung Health Dis. 2019;3(2):31–5.
12. Yang ZC, Yi MJ, Ran N, Wang C, Fu P, Feng XY, et al. Transforming growth factor-beta1 induces bronchial epithelial cells to mesenchymal transition by activating the Snail pathway and promotes airway remodeling in asthma. Mol Med Rep. 2013;8(6):1663–8.
13. Willis BC, Liebler JM, Luby-Phelps K, Nicholson AG, Crandall ED, du Bois RM, Borok Z. Induction of epithelial-mesenchymal transition in alveolar epithelial cells by transforming growth factor-beta1: potential role in idiopathic pulmonary fibrosis. Am J Pathol. 2005;166(5):1321–32.
14. Doerner AM, Zuraw BL. TGF-beta1 induced epithelial to mesenchymal transition (EMT) in human bronchial epithelial cells is enhanced by IL-1beta but not abrogated by corticosteroids. Respir Res. 2009;10(1):100.
15. Yao L, Xu Z, Davies DE, Jones MG, Wang Y. Dysregulated bidirectional epithelial-mesenchymal crosstalk: a core determinant of lung fibrosis progression. Chin Med J Pulm Crit Care Med. 2024;2(1):27–33.
16. Yao L, Zhou Y, Li J, Wickens L, Conforti F, Rattu A, et al. Bidirectional epithelial-mesenchymal crosstalk provides self-sustaining profibrotic signals in pulmonary fibrosis. J Biol Chem. 2021;297(3):101096.
17. Kasai H, Allen JT, Mason RM, Kamimura T, Zhang Z. TGF-beta1 induces human alveolar epithelial to mesenchymal cell transition (EMT). Respir Res. 2005;6(1):56.
18. Luo L, Zhang W, You S, Cui X, Tu H, Yi Q, et al. The role of epithelial cells in fibrosis: Mechanisms and treatment. Pharmacol Res. 2024;202:107144.
19. Lovisa S. Epithelial-to-Mesenchymal Transition in Fibrosis: Concepts and Targeting Strategies. Front Pharmacol. 2021;12:737570.
20. Sato N, Takasaka N, Yoshida M, Tsubouchi K, Minagawa S, Araya J, et al. Metformin attenuates lung fibrosis development via NOX4 suppression. Respir Res. 2016;17(1):107.
21. Rangarajan S, Bone NB, Zmijewska AA, Jiang S, Park DW, Bernard K, et al. Metformin reverses established lung fibrosis in a bleomycin model. Nat Med. 2018;24(8):1121–7.
22. Mishra R, Cool BL, Laderoute KR, Foretz M, Viollet B, Simonson MS. AMP-activated protein kinase inhibits transforming growth factor-beta-induced Smad3-dependent transcription and myofibroblast transdifferentiation. J Biol Chem. 2008;283(16):10461–9.
23. Cheng D, Xu Q, Wang Y, Li G, Sun W, Ma D, et al. Metformin attenuates silica-induced pulmonary fibrosis via AMPK signaling. J Transl Med. 2021;19(1):349.
24. Lizcano JM, Goransson O, Toth R, Deak M, Morrice NA, Boudeau J, et al. LKB1 is a master kinase that activates 13 kinases of the AMPK subfamily, including MARK/PAR-1. EMBO J. 2004;23(4):833–43.
25. Zhang Y, Meng Q, Sun Q, Xu ZX, Zhou H, Wang Y. LKB1 deficiency-induced metabolic reprogramming in tumorigenesis and non-neoplastic diseases. Mol Metab. 2021;44:101131.
26. Shaw RJ, Kosmatka M, Bardeesy N, Hurley RL, Witters LA, DePinho RA, Cantley LC. The tumor suppressor LKB1 kinase directly activates AMP-activated kinase and regulates apoptosis in response to energy stress. Proc Natl Acad Sci U S A. 2004;101(10):3329–35.
27. Mihaylova MM, Shaw RJ. The AMPK signalling pathway coordinates cell growth, autophagy and metabolism. Nat Cell Biol. 2011;13(9):1016–23.
28. Xu Z, Davies ER, Yao L, Zhou Y, Li J, Alzetani A, et al. LKB1 depletion-mediated epithelial-mesenchymal transition induces fibroblast activation in lung fibrosis. Genes Dis. 2024;11(3):101065.
29. Roy BC, Kohno T, Iwakawa R, Moriguchi T, Kiyono T, Morishita K, et al. Involvement of LKB1 in epithelial-mesenchymal transition (EMT) of human lung cancer cells. Lung Cancer. 2010;70(2):136–45.
30. Herrmann JL, Byekova Y, Elmets CA, Athar M. Liver kinase B1 (LKB1) in the pathogenesis of epithelial cancers. Cancer Lett. 2011;306(1):1–9.
31. Zhu XN, He P, Zhang L, Yang S, Zhang HL, Zhu D, et al. FBXO22 mediates polyubiquitination and inactivation of LKB1 to promote lung cancer cell growth. Cell Death Dis. 2019;10(7):486.
32. Zhu H, Moriasi CM, Zhang M, Zhao Y, Zou MH. Phosphorylation of serine 399 in LKB1 protein short form by protein kinase Czeta is required for its nucleocytoplasmic transport and consequent AMP-activated protein kinase (AMPK) activation. J Biol Chem. 2013;288(23):16495–505.
33. Xie Z, Dong Y, Scholz R, Neumann D, Zou MH. Phosphorylation of LKB1 at serine 428 by protein kinase C-zeta is required for metformin-enhanced activation of the AMP-activated protein kinase in endothelial cells. Circulation. 2008;117(7):952–62.
34. Lan F, Cacicedo JM, Ruderman N, Ido Y. SIRT1 modulation of the acetylation status, cytosolic localization, and activity of LKB1. Possible role in AMP-activated protein kinase activation. J Biol Chem. 2008;283(41):27628–35.
35. Borkowsky S, Gass M, Alavizargar A, Hanewinkel J, Hallstein I, Nedvetsky P et al. Phosphorylation of LKB1 by PDK1 Inhibits Cell Proliferation and Organ Growth by Decreased Activation of AMPK. Cells. 2023;12(5):812.
36. Bian T, Wang Y, Botello JF, Hu Q, Jiang Y, Zingone A, et al. LKB1 phosphorylation and deactivation in lung cancer by NNAL, a metabolite of tobacco-specific carcinogen, in an isomer-dependent manner. Oncogene. 2022;41(33):4042–54.
37. Wolf E, Vassilev A, Makino Y, Sali A, Nakatani Y, Burley SK. Crystal structure of a GCN5-related N-acetyltransferase: Serratia marcescens aminoglycoside 3-N-acetyltransferase. Cell. 1998;94(4):439–49.
38. Sun J, Paduch M, Kim SA, Kramer RM, Barrios AF, Lu V, et al. Structural basis for activation of SAGA histone acetyltransferase Gcn5 by partner subunit Ada2. Proc Natl Acad Sci U S A. 2018;115(40):10010–5.
39. Zhang W, Guo X, Ren J, Chen Y, Wang J, Gao A. GCN5-mediated PKM2 acetylation participates in benzene-induced hematotoxicity through regulating glycolysis and inflammation via p-Stat3/IL17A axis. Environ Pollut. 2022;295:118708.
40. Xiao HT, Jin J, Zheng ZG. Emerging role of GCN5 in human diseases and its therapeutic potential. Biomed Pharmacother. 2023;165:114835.
41. Cho DY, Han JH, Kim IS, Lim JH, Ko HM, Kim B, Choi DK. The acetyltransferase GCN5 contributes to neuroinflammation in mice by acetylating and activating the NF-kappaB subunit p65 in microglia. Sci Signal. 2025;18(876):eadp8973.
42. Henderson WR Jr., Chi EY, Ye X, Nguyen C, Tien YT, Zhou B, et al. Inhibition of Wnt/beta-catenin/CREB binding protein (CBP) signaling reverses pulmonary fibrosis. Proc Natl Acad Sci U S A. 2010;107(32):14309–14.
43. Tao J, Zhang M, Wen Z, Wang B, Zhang L, Ou Y, et al. Inhibition of EP300 and DDR1 synergistically alleviates pulmonary fibrosis in vitro and in vivo. Biomed Pharmacother. 2018;106:1727–33.
44. Rubio K, Singh I, Dobersch S, Sarvari P, Gunther S, Cordero J, et al. Inactivation of nuclear histone deacetylases by EP300 disrupts the MiCEE complex in idiopathic pulmonary fibrosis. Nat Commun. 2019;10(1):2229.
45. Wang L, Lin F, Liu J, Jia Z, Zhu M, Liu Y, et al. Revealing a new target: Celastrol alleviates pulmonary fibrosis by inhibiting PCAF. Bioorg Chem. 2025;163:108722.
46. Lee SY, Park SY, Lee SH, Kim H, Kwon JH, Yoo JY, et al. The deubiquitinase UCHL3 mediates p300-dependent chemokine signaling in alveolar type II cells to promote pulmonary fibrosis. Exp Mol Med. 2023;55(8):1795–805.
47. Lee CG, Cho SJ, Kang MJ, Chapoval SP, Lee PJ, Noble PW, et al. Early growth response gene 1-mediated apoptosis is essential for transforming growth factor beta1-induced pulmonary fibrosis. J Exp Med. 2004;200(3):377–89.
48. Abramson J, Adler J, Dunger J, Evans R, Green T, Pritzel A, et al. Accurate structure prediction of biomolecular interactions with AlphaFold 3. Nature. 2024;630(8016):493–500.
49. van Zundert GCP, Rodrigues J, Trellet M, Schmitz C, Kastritis PL, Karaca E, et al. The HADDOCK2.2 Web Server: User-Friendly Integrative Modeling of Biomolecular Complexes. J Mol Biol. 2016;428(4):720–5.
50. van Dijk M, van Dijk AD, Hsu V, Boelens R, Bonvin AM. Information-driven protein-DNA docking using HADDOCK: it is a matter of flexibility. Nucleic Acids Res. 2006;34(11):3317–25.
51. Vangone A, Bonvin AM. Contacts-based prediction of binding affinity in protein-protein complexes. Elife. 2015;4:e07454.
52. Cecchini MJ, Hosein K, Howlett CJ, Joseph M, Mura M. Comprehensive gene expression profiling identifies distinct and overlapping transcriptional profiles in non-specific interstitial pneumonia and idiopathic pulmonary fibrosis. Respir Res. 2018;19(1):153.
53. Sikkema L, Ramirez-Suastegui C, Strobl DC, Gillett TE, Zappia L, Madissoon E, et al. An integrated cell atlas of the lung in health and disease. Nat Med. 2023;29(6):1563–77.
54. Lan F, Lin Y, Gao Z, Cacicedo JM, Weikel K, Ido Y. Activation of LKB1 rescues 3T3-L1 adipocytes from senescence induced by Sirt1 knock-down: a pivotal role of LKB1 in cellular aging. Aging. 2020;12(19):18942–56.
55. Shukri AH, Lukinovic V, Charih F, Biggar KK. Unraveling the battle for lysine: A review of the competition among post-translational modifications. Biochim Biophys Acta Gene Regul Mech. 2023;1866(4):194990.
56. Ali I, Conrad RJ, Verdin E, Ott M. Lysine Acetylation Goes Global: From Epigenetics to Metabolism and Therapeutics. Chem Rev. 2018;118(3):1216–52.

57. Wang Y, Huang Y, Liu J, Zhang J, Xu M, You Z, et al. Acetyltransferase GCN5 regulates autophagy and lysosome biogenesis by targeting TFEB. EMBO Rep. 2020;21(1):e48335.
58. Mutlu B, Puigserver P. GCN5 acetyltransferase in cellular energetic and metabolic processes. Biochim Biophys Acta Gene Regul Mech. 2021;1864(2):194626.
59. Haque ME, Jakaria M, Akther M, Cho DY, Kim IS, Choi DK. The GCN5: its biological functions and therapeutic potentials. Clin Sci (Lond). 2021;135(1):231–57.
60. Alessi DR, Sakamoto K, Bayascas JR. LKB1-dependent signaling pathways. Annu Rev Biochem. 2006;75:137–63.
61. Zeqiraj E, Filippi BM, Deak M, Alessi DR, van Aalten DM. Structure of the LKB1-STRAD-MO25 complex reveals an allosteric mechanism of kinase activation. Science. 2009;326(5960):1707–11.
62. Wynn TA. Integrating mechanisms of pulmonary fibrosis. J Exp Med. 2011;208(7):1339–50.
63. Kage H, Borok Z. EMT and interstitial lung disease: a mysterious relationship. Curr Opin Pulm Med. 2012;18(5):517–23.
64. Niayesh-Mehr R, Kalantar M, Bontempi G, Montaldo C, Ebrahimi S, Allameh A, et al. The role of epithelial-mesenchymal transition in pulmonary fibrosis: lessons from idiopathic pulmonary fibrosis and COVID-19. Cell Commun Signal. 2024;22(1):542.
65. Bridges JP, Vladar EK, Kurche JS, Krivoi A, Stancil IT, Dobrinskikh E et al. Progressive lung fibrosis: reprogramming a genetically vulnerable bronchoalveolar epithelium. J Clin Invest. 2025;135(1):e183836.
66. Hill C, Li J, Liu D, Conforti F, Brereton CJ, Yao L, et al. Autophagy inhibition-mediated epithelial-mesenchymal transition augments local myofibroblast differentiation in pulmonary fibrosis. Cell Death Dis. 2019;10(8):591.
67. Long JK, Dai W, Zheng YW, Zhao SP. miR-122 promotes hepatic lipogenesis via inhibiting the LKB1/AMPK pathway by targeting Sirt1 in non-alcoholic fatty liver disease. Mol Med. 2019;25(1):26.
68. Liu C, Wang X, Wang X, Zhang Y, Min W, Yu P, et al. A new LKB1 activator, piericidin analogue S14, retards renal fibrosis through promoting autophagy and mitochondrial homeostasis in renal tubular epithelial cells. Theranostics. 2022;12(16):7158–79.
69. Liu B, Zhang Y, Wang Y, Meng Q, Zhang D, Yang H, et al. Pharmacological targeting of AMPK to restore glucose and fatty acid metabolism homeostasis attenuates transplanted kidney fibrosis. Biochim Biophys Acta Mol Basis Dis. 2025;1871(1):167510.
70. Bai T, Yang Y, Wu YL, Jiang S, Lee JJ, Lian LH, Nan JX. Thymoquinone alleviates thioacetamide-induced hepatic fibrosis and inflammation by activating LKB1-AMPK signaling pathway in mice. Int Immunopharmacol. 2014;19(2):351–7.
71. Kim H, Park SY, Lee SY, Kwon JH, Byun S, Ko B et al. Loss of p300 in proximal tubular cells reduces renal fibrosis and endothelial-mesenchymal transition. EMBO Mol Med. 2025;17(7):1575–98.
72. Dou C, Liu Z, Tu K, Zhang H, Chen C, Yaqoob U, et al. P300 Acetyltransferase Mediates Stiffness-Induced Activation of Hepatic Stellate Cells Into Tumor-Promoting Myofibroblasts. Gastroenterology. 2018;154(8):2209–e2114.
73. Kim H, Kwon JH, Lee SH, Byun S, Kim H, Kim HS et al. Loss of PCAF in proximal tubular cells exacerbates renal fibrosis by promoting partial epithelial-to-mesenchymal transition. Exp Mol Med. 2025;57(9):2010–21.
74. Ouyang C, Mu J, Lu Q, Li J, Zhu H, Wang Q, et al. Autophagic degradation of KAT2A/GCN5 promotes directional migration of vascular smooth muscle cells by reducing TUBA/alpha-tubulin acetylation. Autophagy. 2020;16(10):1753–70.
75. Jeong DS, Kim YC, Oh JH, Kim MH. Akt1 Decreases Gcn5 Protein Stability through Regulating The Ubiquitin-Proteasome Pathway in Mouse Embryonic Fibroblasts. Cell J. 2022;24(1):51–4.

Publisher's note